

Micro-Raman Spectroscopy of Particles in the Mie-size Range: A Short Review

W. Kiefer

*Institut für Physikalische Chemie der Universität Würzburg, Marcusstr. 9—11,
D-8700 Würzburg, F. R. Germany*

Received April 20, 1988

In this paper a short review is given on micro-Raman spectroscopy where the particles or the dimensions of scattering systems under investigation are comparable to the wavelength of the exciting laser light. If the scattering system has well-defined geometries, e.g. spheres, cylinders, etc., structural resonances can be observed in inelastical light scattering experiments. These resonances can be explained by the well-known Lorenz-Mie-theory. Examples of such Raman-Mie spectra of solid and liquid microspheres, as well as of fibers, are given. A variety of laser light traps are discussed which allow to study such Raman-Mie spectra experimentally.

1. INTRODUCTION

In linear Raman spectroscopy of bulk samples, the energy shift of the peaks in a Raman spectrum can be ascribed to a specific molecular vibration and the intensity of each peak is linearly proportional to the concentration of the specific molecule and the Raman scattering cross section of the particular vibrational transition. Recent technical advances made it possible to obtain Raman spectra of samples whose sizes are of the order of or larger than the wavelength of the exciting light. However, if such small scattering systems have well defined geometries, e.g. spheres, cylinders, spheroids, etc., the use of Raman spectroscopy as a diagnostic probe becomes much more complicated as a result of morphology-dependent resonances. Such resonances can actually give rise to sharp peaks in a Raman spectrum that are not present for a bulk sample of the same composition. These peaks can result from resonance-induced enhancement of the Raman scattering or of the enhancement of a fluorescence background. The physical nature of these resonances can be described for dielectric particles by means of the well-known Lorenz-Mie theory. If misinterpreted, such resonance-induced peaks could lead to confusion in analyzing Raman spectra. The purpose of this paper is to emphasize this point and to review achievements in the investigation and interpretation of Raman spectra taken from microparticles or scattering systems with well defined geometry in the Mie-size range. We will outline the appropriate theory for morphology-dependent resonances, describe shortly experimental situations, where such »Raman-Mie«-spectra are to be observed and finally give some examples of this kind of spectra.

2. THEORY OF MORPHOLOGY DEPENDENT RESONANCES

Since morphology-dependent resonances manifest themselves in elastic scattering, we first have to consider this type of light scattering.

For dielectric spheres with radius a and an incident plane wave of wavelength λ , we first have to apply the Lorenz-Mie formalism in order to calculate the size parameter $x = 2\pi a/\lambda$ at which peaks will exist in an elastic scattering spectrum¹⁻³. The scattering efficiency Q_s which is a measure of the ability of a sphere to capture power from the incident plane wave and redirect it as scattered power, is given by¹

$$Q_s = \frac{2}{x^2} \sum_{n=1}^{\infty} (2n+1) (|a_n|^2 + |b_n|^2) \quad (1)$$

where the expansion coefficients a_n and b_n are given by¹

$$a_n = \frac{j_n(x) [mxj_n(mx)]' - m^2 j_n(mx) [xj_n(x)]'}{h_n^{(2)}(x) [mxj_n(mx)]' - m^2 j_n(mx) [xh_n^{(2)}(x)]'} \quad (2)$$

and

$$b_n = \frac{j_n(x) [mxj_n(mx)]' - j_n(mx) [xj_n(x)]'}{h_n^{(2)}(x) [mxj_n(mx)]' - j_n(mx) [xh_n^{(2)}(x)]'} \quad (3)$$

where m is the relative refractive index and j_n and $h_n^{(2)}$ are the spherical Bessel functions and Hankel functions of the second kind, respectively. The primes denote differentiation with respect to the argument of the function. Coefficients a_n and b_n show resonance behavior and each of them can be associated with a structural mode of electromagnetic vibration of the sphere.³

The calculated scattering efficiency as a function of size parameter is shown in Figure 1 for a dielectric sphere with an index of refraction of 1.500 for field A and 1.577 for all other fields, respectively. Fields C and D are expanded views of field B over a narrow size-parameter range. The detailed behavior of the rapid oscillation can be seen in particular in the expanded views. There, one notices further the fine structure consisting of narrow peaks on the rapid oscillations which were seen in field A. The peaks in field D (both narrow and broad) are a manifestation of the resonance behavior of the a_n and b_n coefficients given in Eqs. 2 and 3. Each of these coefficients can be associated with a structural mode of electromagnetic vibration of the dielectric sphere. In field D we have labelled the peaks according to the coefficient that is responsible for the resonance. The subscript n and the superscript l denote the l th resonance of the n th mode. For example, a_{168}^3 is the third peak at the 168 coefficient as x increases from zero.

Similarly to the a_n and b_n coefficients, which correspond to the TM and TE modes of the scattered field, respectively, the c_n and d_n coefficients (TM and TE modes of the internal field, respectively), defined by²

$$c_n = \frac{mi/x}{h_n^{(2)}(x) [mxj_n(mx)]' - m^2 j_n(mx) [xh_n^{(2)}(x)]'} \quad (4)$$

and

$$d_n = \frac{i/x}{h_n^{(2)}(x) [mxj_n(mx)]' - j_n(mx) [xh_n^{(2)}(x)]'} \quad (5)$$

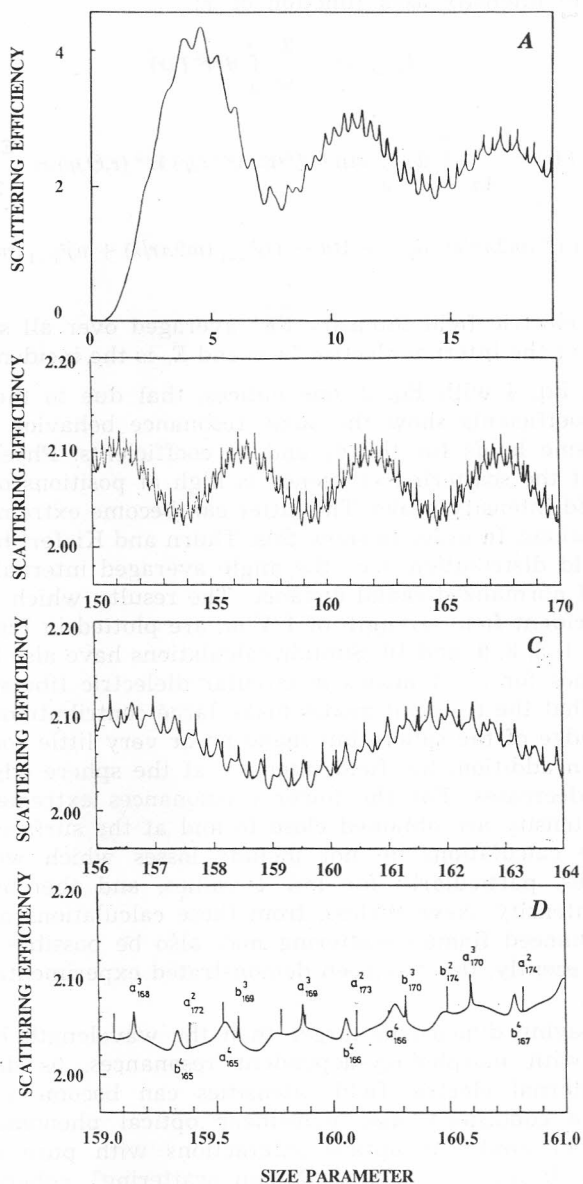


Figure 1. Scattering efficiency versus size parameter for a dielectric sphere of refractive index $m = 1.500$ (field A) and $m = 1.577$ (fields B—D). Fields C and D are expanded views of B over a narrow size-parameter range. The n subscripts and the l superscripts indicate the mode and the order of each resonance, respectively.

$$I_{\text{total}}(x) = \frac{3}{a^3} \int_0^a dr r^2 I(r) \quad (6)$$

where

$$I(r) = \frac{1}{4\pi} \int_0^{2\pi} d\varphi \int_0^\pi \sin\Theta d\Theta \mathbf{E}^i(r, \Theta, \varphi) \mathbf{E}^{i*}(r, \Theta, \varphi) = \frac{E_0^2}{2} \cdot$$

$$\sum_{n=1}^{\infty} \{ (2n+1) j_n^2(m2\pi r/\lambda) |d_n|^2 + [(n+1)j_{n-1}^2(m2\pi r/\lambda) + nj_{n+1}^2(m2\pi r/\lambda)] |c_n|^2 \} \quad (7)$$

is the internal electric field intensity $\overline{EE^*}$ averaged over all spherical angles. \mathbf{E}^i is the vector of the internal electric field and E_0 is the incident field strength.

Comparing Eq. 4 with Eq. 2, one notices, that due to the same denominator, the c_n coefficients show the same resonance behavior as the a_n coefficients. The same holds for the d_n and b_n coefficients. Physically speaking, this means, that the scattering efficiency is high at positions of x , where also the internal field intensity peaks. The latter can become extremely large under resonance conditions. In order to show this, Thurn and Kiefer⁴ have determined the internal field distribution, i. e., the angle averaged internal field intensity as a function of normalized radial distance. The results, which were calculated assuming an incident field strength of 1 V/m, are plotted in Figure 2. for TE_{154} modes with $l = 1, 5, 8, 9$, and 10. Similar calculations have also been performed at lower x values for $l = 1$ modes in circular dielectric fibers⁵ and dielectric spheres⁶. Note that the resonant modes make large contributions to the electric field near the edge of the sphere but make no or very little contribution close to the center. In addition, the field intensity at the sphere edge dramatically increases as l decreases. For the lower l resonances extremely high values for the field intensity are obtained close to and at the surface of the sphere. However, these calculations do not include losses which would damp the structural modes, particularly for low l values, and thereby decrease the internal field intensity. Nevertheless, from these calculations one can assume, that surface-enhanced Raman scattering may also be possible on nonmetallic surfaces. Very recently, this has been demonstrated experimentally by Hayashi *et al.*⁷

A sphere having dimensions larger than the wavelength behaves like an optical cavity with morphology-dependent resonances, as discussed above. Because the internal electric field intensities can become extremely large under resonance conditions, also non-linear optical phenomena can occur. Recent reports of nonlinear optical interactions with pure or dyed liquid droplets include lasing,⁸ stimulated Raman scattering⁹, coherent anti-Stokes Raman scattering (CARS)¹⁰, and coherent Raman mixing¹⁰. Multiorder Stokes emission from micrometer-size droplets of CCl_4 were reported recently¹¹. The stimulated Raman scattering from such droplets exhibited up to the fourteenth-order Stokes peaks and multiorder combination Stokes emission without detectable anti-Stokes emission. These results could also be explained by the morphology-dependent resonances of the droplet which acts as an optical

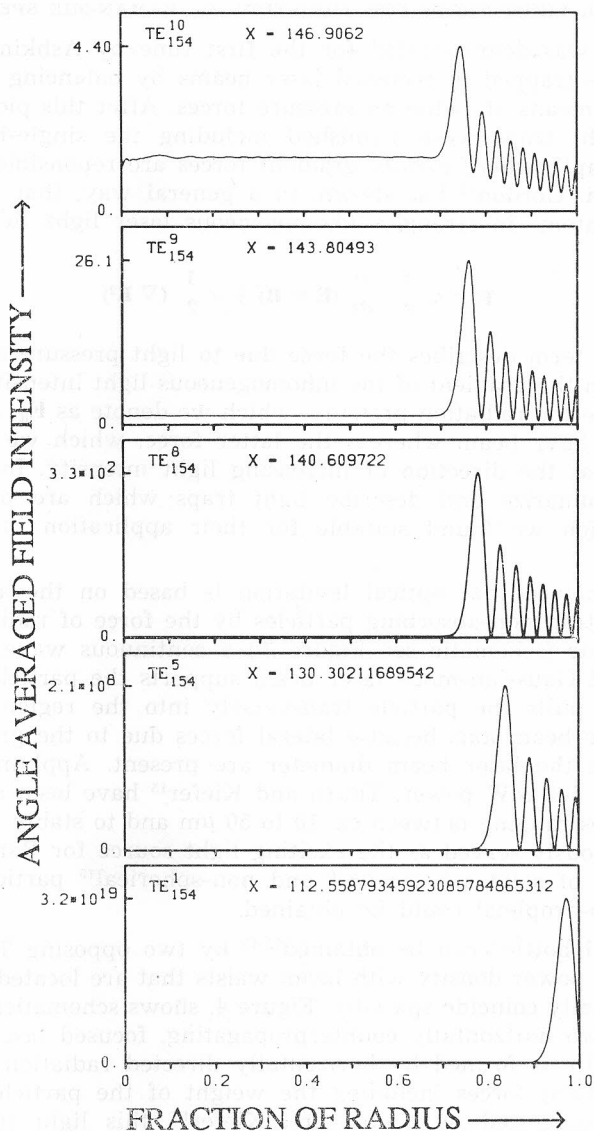


Figure 2. Calculated angle averaged field intensity within a lossless dielectric sphere as a function of the fraction of radius. Calculations are shown for $m = 1.45$ and x satisfying resonance conditions for TE_{154} modes (Ref. 4).

cavity, providing high optical feedback and supporting enhanced internal fields at various Stokes shifts¹¹.

Studies of the structural resonances and internal electric field distributions have been carried out also for dielectric cylinders with micrometer-size diameter⁵. The electromagnetic solution for the circular cylinder parallels that for the sphere⁵.

3. LASER LIGHT TRAPS FOR THE STUDY OF RAMAN-MIE SPECTRA

In 1970, it was demonstrated for the first time by Ashkin¹² that micro-particles can be trapped in focussed laser beams by balancing the weight of the particle by means of radiation pressure forces. After this pioneering work, some other light traps were published including the single-beam gradient force optical trap¹³, where mainly gradient forces are responsible for the trapping mechanism. Gordon¹⁴ has shown, in a general way, that dielectric particles or even atoms in strongly inhomogeneous laser light fields undergo a total force

$$\mathbf{F} = \alpha \frac{1}{c} \frac{\partial}{\partial t} (\mathbf{E} \times \mathbf{B}) + \alpha \frac{1}{2} (\nabla E^2) \quad (8)$$

where the first term describes the force due to light pressure and the second one results from the gradient of the inhomogeneous light intensity distribution. The force due to the radiation pressure, which we denote as \mathbf{F}_R , has a direction parallel to the laser beam whereas the latter force, which we call »gradient force« (\mathbf{F}_{grad}), has the direction of increasing light intensity. In the following we shortly summarize and describe light traps which are based on these forces and which we found suitable for their application in micro-Raman spectroscopy.

Ashkin¹² showed that optical levitation is based on the ability of laser light to stably trap non-absorbing particles by the force of radiation pressure. In this technique (schematic see Figure 3.) a continuous wave, vertically directed, focussed Gaussian-mode laser beam supports the particle's weight and simultaneously pulls the particle transversely into the region of high light intensity on the beam axis because lateral forces due to the gradient in light intensity across the laser beam diameter are present. Applying a cw argon ion laser of ca. 500 mW power, Thurn and Kiefer¹⁵ have been able to levitate particles of sizes ranging between ca. 10 to 50 μm and to stably trap them. The laser simultaneously served as the exciting light source for Raman scattering. Raman spectra of solid spherical^{15,16} and non-spherical¹⁵ particles as well as of liquid micro-droplets⁴ could be obtained.

An »optical bottle« can be obtained^{12,15} by two opposing TEM_{00} Gaussian beams of equal power density with beam waists that are located close together but do not actually coincide spatially. Figure 4. shows schematically this arrangement with two horizontally counterpropagating, focused laser beams. Here, the optical bottle is formed by horizontally directed radiation forces and by the radial gradient forces including the weight of the particle, as shown in Figure 4. As suggested by Thurn and Kiefer¹⁵, this light trap allows the observation of inelastically scattered light from very small particles.

Recently, Ashkin *et al.*¹³ have shown that optical trapping of dielectric particles can be achieved by a single beam gradient force trap. The latter confirms the concept of negative light pressure due to the gradient force. The principle of this laser light trap is schematically outlined in Figure 5. A strongly focused laser beam, e. g. with an 100 fold microscope objective, generates a high spatially inhomogeneous laser light field, which itself gives rise to strong gradient forces not only in a lateral direction but also in the direction along the laser beam axis. As a consequence, the particle can be trapped at a position slightly below the beam waist, when the laser beam comes vertically

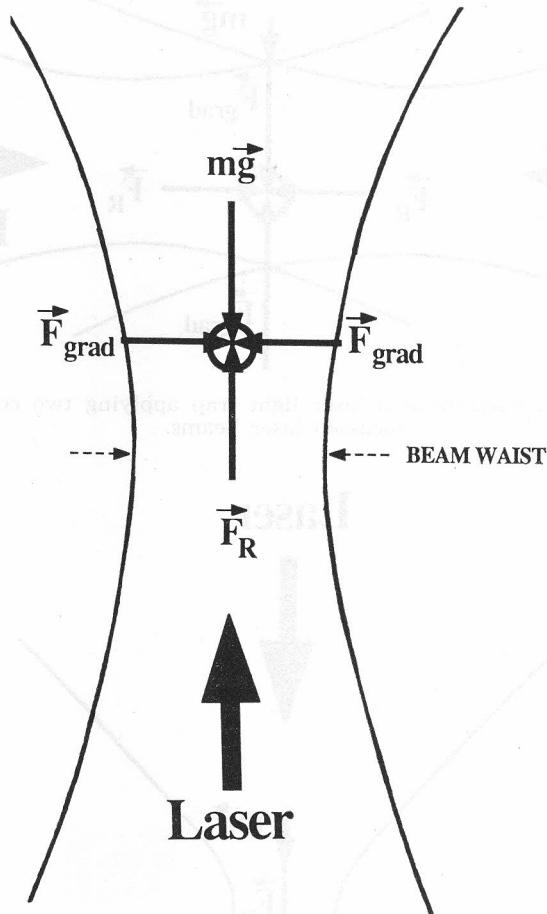


Figure 3. Schematic diagram of the optical levitation by radiation technique. F_R and F_{grad} are radiation and gradient forces, respectively.

from above. The force equilibrium is performed by an upwards directed gradient force, which is balanced by the sum of the particle weight and the radiation force of the laser beam. If, again, a laser beam with Gaussian beam profile is employed, the lateral force balance is achieved by gradient forces, as schematically shown in Figure 5.

Ashkin *et al.*¹³ observed trapping over the entire range of particle size from 10 μm to ~ 25 nm in water. Use of this new laser light trap well extends the size range of macroscopic particles accessible to optical trapping into the Rayleigh size regime. We have been able to stably trap glass spheres in the size range from ~ 10 to 1 μm .¹⁷ Such a laser light trap can also be used for the investigation of particles in liquids, like living cells or bacteria in water. In the first attempt we were successful in trapping single *E. coli* bacteria.

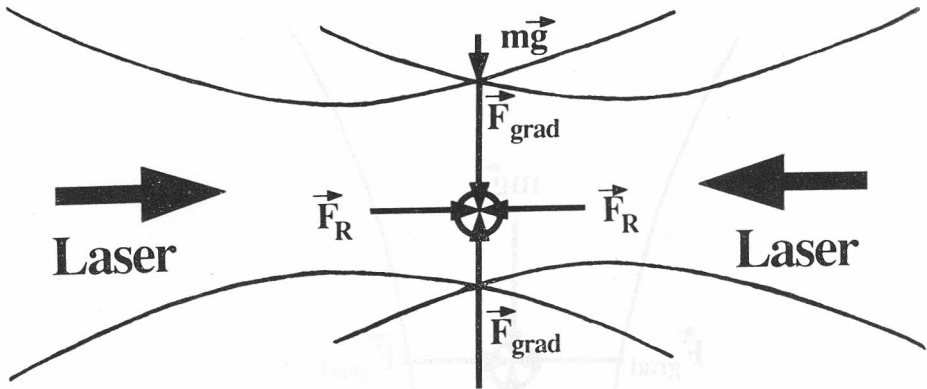


Figure 4. Schematic diagram of a laser light trap applying two counterpropagating focussed laser beams.

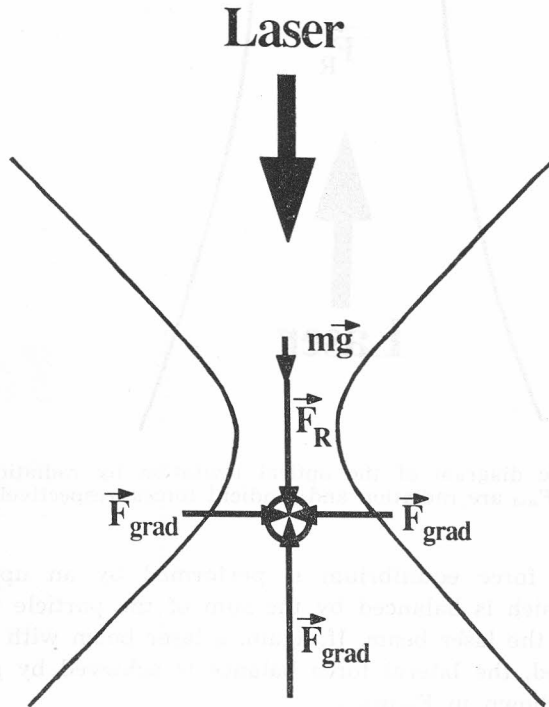


Figure 5. The single-beam gradient force optical trap.

4. RAMAN-MIE SPECTRA OF MICROPARTICLES AND FIBERS

In this chapter some typical Raman spectra of samples are shown, whose geometry is such that structural resonances can occur (*»Raman-Mie-spectra«*). The samples selected are: (i) a solid glass microsphere, (ii) a microdroplet, and (iii) a fiber, whose diameter is in the micronrange.

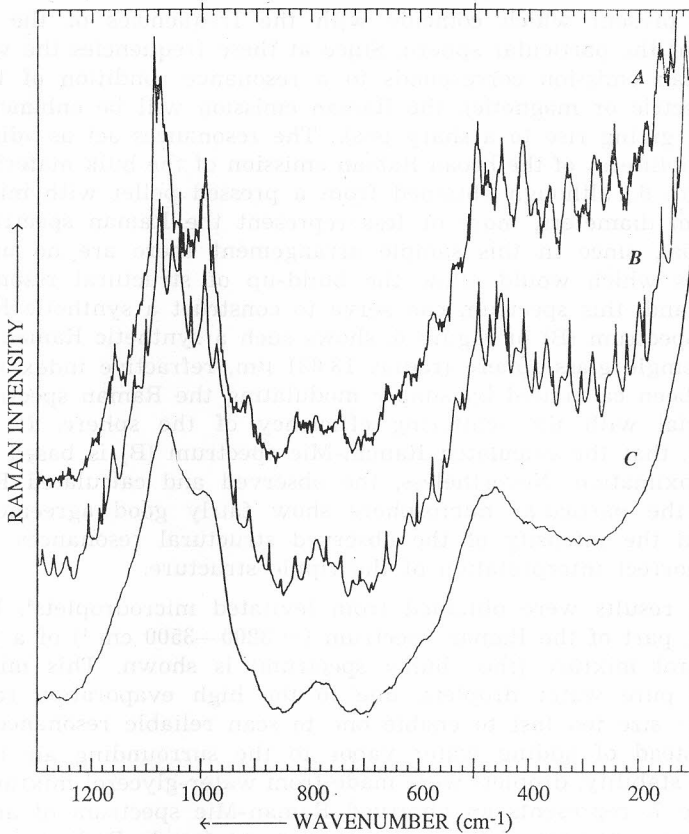


Figure 6. Experimentally observed Raman-Mie spectrum of an optically levitated glass sphere of diameter $27 \mu\text{m}$ (A). The spectrum displayed in (B) is a theoretically calculated Raman spectrum applying the Lorenz-Mie formalism and the lower spectrum (C) is a Raman spectrum of a pressed pellet of glass spheres, with diameter ranging between 0.5 and $35 \mu\text{m}$. (Ref. 16).

Figure 6. shows the experimentally observed Raman-Mie spectrum¹⁶ (A) from an optically levitated glass sphere with a diameter of ca $27 \mu\text{m}$ and a refractive index of 1.56. Part (C) of Figure 6. shows a Raman spectrum of a pellet of the same glass material but with random diameters ranging between 0.5 and $35 \mu\text{m}$. The relatively broad Raman lines in the spectrum of the pellet at about 500 and 1100 cm^{-1} are also well represented in the spectrum of the single microsphere. Comparison of the spectra (A) and (C) in Figure 6. reveals that the general features of the Raman spectrum of the single microsphere are well reproduced. However, in addition, one observes a regular structure of sharp peaks in the spectrum of the micro-sized sphere. This ripple structure, which is very pronounced in the spectral region between about 200 and 500 cm^{-1} and between about 900 and 1200 cm^{-1} is due to the structural resonances initiated by the Raman light generated inside the glass sphere. Since the Raman spectrum of the glass is essentially continuous in the region of interest (see spectrum C in Figure 6.), there are always electromagnetic

frequencies present which coincide with the frequencies of the structural resonances of the particular sphere. Since at these frequencies the wavelength of the Raman emission corresponds to a resonance condition of the micro-particle (electric or magnetic), the Raman emission will be enhanced at that wavelength, giving rise to a sharp peak. The resonances act as »discrete wavelength amplifiers« of the broad Raman emission of the bulk material¹⁸. Trace (C) of Figure 6., although obtained from a pressed pellet with microspheres with random diameters, more or less represent the Raman spectrum of the bulk material, since in this sample arrangement there are no undisturbed microspheres which would allow the build-up of structural resonances. On the other hand, this spectrum can serve to construct a synthetic Raman-Mie spectrum. Spectrum (B) of Figure 6. shows such a synthetic Raman-Mie spectrum of a single glass sphere (radius 13.831 μm , refractive index $m = 1.577$), which has been calculated by simply modulating the Raman spectrum of the bulk material with the scattering efficiency of the sphere. It should be pointed out, that the calculated Raman-Mie spectrum (B) is based on a very crude approximation. Nevertheless, the observed and calculated Raman-Mie spectra of the particular microsphere show fairly good agreement in the position and the intensity of the observed structural resonances and hence prove the correct interpretation of the ripple structure.

Similar results were obtained from levitated microdroplets⁴. In field A of Figure 7. part of the Raman spectrum ($\sim 3200\text{--}3500\text{ cm}^{-1}$) of a liquid 1:6 water-glycerol mixture (the »bulk« spectrum) is shown. This mixture was used, since pure water droplets, due to the high evaporation rate in air, change their size too fast to enable one to scan reliable resonance structure spectra. Instead of adding water vapor to the surrounding air to increase droplet size stability, droplets were made from water-glycerol mixtures⁴. Curve B of Figure 7. represents an observed Raman-Mie spectrum of an optically levitated single droplet of the same mixture as for A. Radius a of this dielectric sphere is $\sim 15 \pm 1\ \mu\text{m}$ as measured with a microscope. In field C a theoretically calculated Raman-Mie spectrum is shown, which can be expected for a dielectric sphere of refractive index $m = 1.45$, and a radius of $a = 14.422\ \mu\text{m}$, if the Lorenz-Mie formalism is applied and only the higher resonances ($l = 8$ and 9) of the modes are taken into consideration. For details in the calculation see Reference 4. Again, the agreement between experimental and calculated Raman-Mie spectra is reasonable. The fact that only modes of quite high order ($l = 8$ and 9) are observed needs some discussion. The lower the order l of a resonance, the narrower the linewidth of the structural resonance peak and the larger the internal fields associated with the resonance, i. e. the higher the Q of the resonance. Because of the high Q , the lower-order resonances tend to be damped by imperfections of the microsphere (e. g., surface irregularity, focussing and heating effects of the laser radiation, mechanical oscillations of the sphere, etc.). Therefore, lower order modes seem to be too unstable for observation.

Finally, we give an example of resonance structure in a fiber. Fibers of silicate glass provide good samples for studying such resonances since Raman lines from SiO_2 are relatively broad compared to structure resonances in a $10\text{-}\mu\text{m}$ -diam fiber. In Figure 8, which has been taken from Reference 18, spectra and calculations for two different excitation frequencies are displayed:

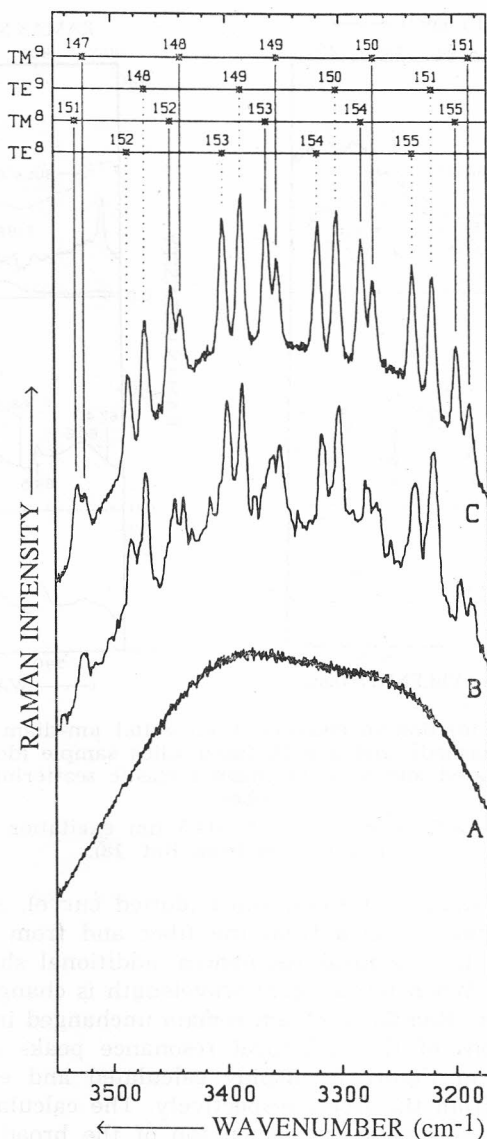


Figure 7. (A): The O—H stretching region of the Raman spectrum of a liquid 1:6 water-glycerol mixture (refractive index $m = 1.45$); (B): Observed Raman-Mie spectrum of a laser-trapped liquid droplet of the same mixture as for A (radius of sphere a ca. $15 \mu\text{m}$); (C): Theoretically calculated Raman-Mie spectrum applying the Lorenz-Mie formalism (Ref. 4).

the left field shows the situation for 488.0 nm and the right field for 514.5 nm excitation, respectively. The upper part (a) shows the Raman spectrum from a $10.1\text{-}\mu\text{m}$ -diam glass fiber (solid curve), the Raman spectrum from a similar, although not identical, bulk glass sample (dashed curve), and the Raman spec-

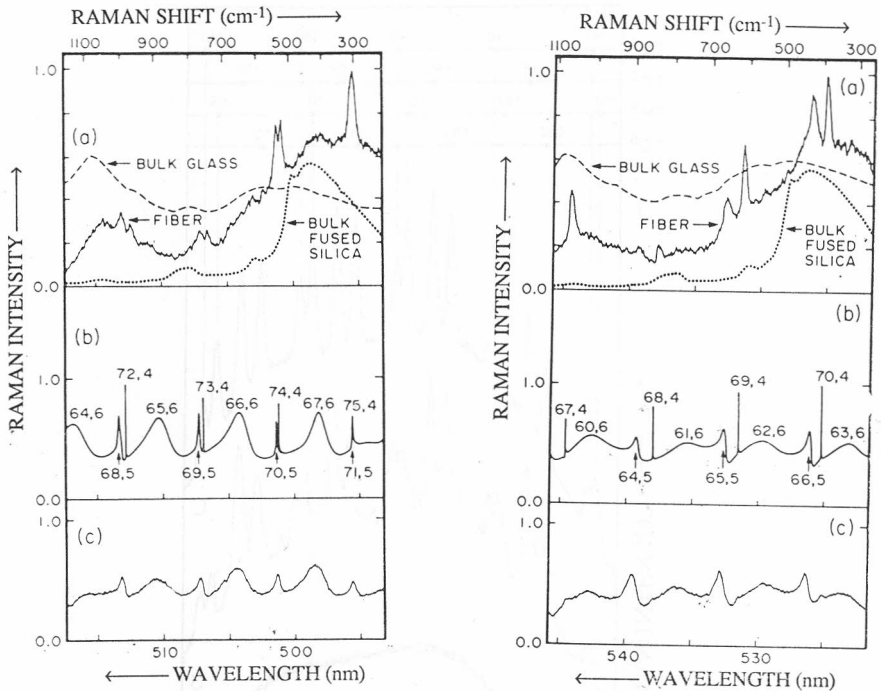


Figure 8. Left field: (a) Raman emission from a 10.1 μm -diam glass fiber (solid), a bulk glass sample (dashed), and a bulk fused silica sample (dotted) using 488.0 nm excitation; (b) calculated and (c) experimental elastic scattering spectrum from the fiber;

Right field: same as left field, but with 514.5 nm excitation of Raman emission. (Reproduced from Ref. 18).

trum from a bulk sample of fused silica (dotted curve). Although the broad features of the Raman spectra from the fiber and from the bulk glass are similar, again, due to structural resonances, additional sharp peaks occur in the fiber spectrum. When the incident wavelength is changed to 514.5 nm, the broad features of the Raman spectrum remain unchanged in energy shift while the relative positions of the structural resonance peaks are quite different. Fields (b) and (c) in Figure 8. display calculated and experimental elastic scattering spectra from the fiber, respectively. The calculations again help to assign the observed resonance peaks on top of the broad Raman bands.

5. CONCLUSIONS

In this paper a short review has been given of a special micro-Raman spectroscopic technique. It was emphasized that, if scattering systems are of the order of or larger than the exciting line, special precaution is necessary when vibrational assignments are carried out. It was shown, that micro-spheres and fibers not only give rise to Raman bands similar to those of the bulk material, but in addition one observes a large number of peaks which arise as a consequence of electromagnetic vibrations of the sphere or of the fiber. Such morphology-dependent (structural) resonances can add sharp structure

to normally broad featureless Raman lines or can greatly distort the line-shapes of Raman peaks with linewidths similar to the widths of the resonances. Fortunately, these distortions only appear in a Raman spectrum of microparticles, if the micro-samples have well defined geometry, e.g. spheres, cylinders, spheroids, which means that the sample acts as an optical resonator with high Q . As was shown by Thurn and Kiefer¹⁵, microcrystals do not show this effect. This was demonstrated¹⁵ with a microcrystal of SiO_2 of the size of approximately 20 μm .

The purpose of this paper was to emphasize the effect that happens when Raman spectra are taken from scattering systems with well defined geometries. The occurrence of such structural resonance modes requires one to take care not to erroneously assign peaks that result from the electromagnetic resonance enhancement to vibrational modes. On the other side, the additional sharp peaks allow one to determine the size of the microparticle with very high accuracy. It is, therefore, possible to use Raman-Mie spectra in order to make studies of size-dependent phenomena, e.g. evaporation of small droplets, condensation on the surface of small spheres, phase transitions in microparticles, etc. The laser light traps described here, can be successfully applied for these purposes.

Acknowledgments. — The author wishes to acknowledge collaboration with R. Thurn (University of Bayreuth, Federal Republic of Germany), P. Knoll and M. Marchl (University of Graz, Austria).

REFERENCES

1. M. Kerker, *The Scattering of Light and Other Electromagnetic Radiation*, Academic Press, New York, 1969, p. 27ff.
2. P. R. Conwell, P. W. Barber, and C. K. Rushfort, *J. Opt. Soc. A* **1** (1984) 62.
3. P. W. Barber, in *Advances in Laser Science — I*, W. C. Stwalley and M. Lapp, Editors, *Am. Inst. Phys. Conf. Proc.* No. 146, New York, 1986, p. 720.
4. R. Thurn and W. Kiefer, *Appl. Opt.* **24** (1985) 1515.
5. J. F. Owen, R. K. Chang, and P. W. Barber, *Opt. Lett.* **6** (1981) 540.
6. P. R. Conwell and P. W. Barber, *J. Opt. Soc. A* **12** (1984) 62.
7. S. Hayashi, R. Koh, Y. Ichiyama, and K. Yamamoto, *Phys. Rev. Lett.* **60** (1988) 1085.
8. H.-M. Tzeng, K. F. Wall, M. B. Long, and R. K. Chang, *Opt. Lett.* **9** (1984) 499.
9. J. B. Snow, S.-X. Qian, and R. K. Chang, *Opt. Lett.* **10** (1985) 37.
10. S.-X. Qian, J. B. Snow, and R. K. Chang, *Opt. Lett.* **10** (1985) 499.
11. S.-X. Qian and R. K. Chang, *Phys. Rev. Lett.* **56** (1986) 926.
12. A. Ashkin, *Phys. Rev. Lett.* **24** (1970) 156.
13. A. Ashkin, J. M. Dziedzic, J. E. Bjorkholm, and S. Chu, *Opt. Lett.* **11** (1986) 288.
14. J. P. Gordon, *Phys. Rev.* **8A** (1973) 14.
15. R. Thurn and W. Kiefer, *Appl. Spectrosc.* **38** (1984) 78.
16. R. Thurn and W. Kiefer, *J. Raman Spectrosc.* **15** (1984) 411.
17. P. Knoll, M. Marchl, and W. Kiefer, *Ind. J. Pure Appl. Phys. (Raman Effect Diamond Jubilee Issue)* **26** (1988) 268.
18. J. F. Owen, R. K. Chang, and P. W. Barber, *Aerosol Sci. Technol.* **1** (1982) 293.

SAŽETAK

Mikro-Ramanova spektroskopija čestica u području Mieove veličine: kratki pregled

W. Kiefer

Dan je kratki pregled mikro-Ramanove spektroskopije, gdje su čestice ili dimenzije ispitivanog sustava za raspršenje usporedive s valnom duljinom pobudne laserske svjetlosti. Ako su sustavi za raspršenje dobro definirani geometrija, npr. kuglice, cilindri i dr., mogu se opaziti strukturne rezonancije u eksperimentima neelastičnog raspršenja svjetlosti. Te se rezonancije mogu objasniti dobro znanom Lorenz-Mieovom teorijom. Prikazani su primjeri ovakvih Raman-Mie-ovih spektara čvrstih i tekućih mikrokuglica, kao i vlakana. Razmatra se čitav niz laserskih svjetlosnih stupica, koje omogućavaju eksperimentalni studij takvih Raman-Mie-ovih spektara.